Geophysical Research Letters

Supporting Information for

How well do we characterize snow storage in High Mountain Asia?

Yufei Liu[1], Yiwen Fang[1], Dongyue Li[1] and Steven A. Margulis[1]

Department of Civil and Environmental Engineering, University of California, Los Angeles, Los Angeles, CA, 90095

Contents of this file

Introduction

This supporting information provides more details on the data, methods and results presented in the main text. Text S1 and Table S1 give details on HMASR and the eight global snow products examined for the intercomparison. Text S2 to Text S6 (along with Table S2 and Figure S1 to Figure S3) provide more clarifications on the methods. Text S7 to Text S9 (along with Table S3 to Table S4; Figure S4 to Figure S6) provide supplementary information for the results.

Text S1. Data: Description of HMASR and eight global snow products

The High Mountain Asia Snow Reanalysis (HMASR) and the eight global snow products are evaluated in this research. Characteristics for each dataset are summarized in Table S1 with details provided as follows:

HMASR (Liu et al., 2021a) is a snow-specific reanalysis dataset, providing daily estimates of SWE at 1/225° (~500 m) resolution, available from Water Years (WYs) 2000 to 2017. Among all datasets examined in this work, HMASR is unique as it was specifically designed for snow estimation in HMA, leveraging remotely sensed fractional snow-covered area (fSCA) and an advanced ensemble-based data assimilation framework. It is directly constrained by snow observations, offering the potential of SWE evaluation at high elevations and over complex terrain, where in-situ stations do not exist.

ERA5 (Hersbach et al., 2020) is the 5th generation product of ECMWF's atmospheric reanalyses that provides hourly estimates at 0.25° resolution. Both in-situ snow depth observations and binary snow cover data from the Interactive Multi-Sensor Snow and Ice Mapping System (IMS) are used in its snow data assimilation (optimal interpolation) system, where snow cover is not used at elevations above 1500 m in the ERA5 snow scheme (Bian et al., 2019). In addition to the ERA5 product itself, the ERA5-land (Muñoz-Sabater et al., 2021) dataset at finer resolution (0.1°) is derived from the same ERA5 forcing and Land Surface model (LSM), but without data assimilation.

MERRA2 (Gelaro et al., 2017) is the 2nd version of NASA's Global Modeling and Assimilation Office (GMAO) reanalysis product, providing hourly estimates at 0.625° x 0.5° resolution. The Catchment model (CLSM) is used as the LSM and no snow data assimilation is performed. MERRA2 uses a bias-corrected precipitation field for precipitation inputs (Reichle et al., 2017) to derive its land surface state estimates including SWE.

JRA55 (Kobayashi et al., 2015) is the latest version of the Japan Meteorology Agency (JMA) reanalysis product that provides sub-daily (e.g. 3-hour snowfall and 6-hour SWE and air temperature) estimates. We selected its highest resolution (~0.5625° x 0.5616°) outputs for this work. JRA55 uses the Simple Biosphere (SiB) model as the LSM in deriving its estimates. Station observed snow depth and satellite retrieved binary snow cover from the Special Sensor Microwave/Imager (SSM/I) and Special Sensor Microwave Imager Sounder (SSMIS) are used to update snow depth using the data assimilation (optimal interpolation) method. SWE estimates are converted from snow depth estimates by assuming a constant snow density (200 kg/m^3; Onogi et al., 2007). The JRA55 product assimilates snow depth data from the stations over the Tibetan Plateau, while ERA5 does not (Onogi et al., 2007; Bian et al., 2019; Orsolini et al., 2019).

GLDAS-2.1 (Rodell et al., 2004) is a global land data assimilation product generated by the NASA Goddard Space Flight Center, providing estimates at sub-daily (3-hour) and 0.25° or 1° resolution, available from January 2000 to present. It contains four datasets: two Noah model driven datasets at 0.25° and 1° resolution, one Variable Infiltration Capacity (VIC) model driven dataset at 1° resolution, and one Catchment (CLSM) model driven dataset at 1° resolution, denoted as GLDAS-Noah (0.25°), GLDAS-Noah (1°), GLDAS-VIC (1°) and GLDAS-CLSM (1°) hereafter. All of the GLDAS-2.1 products are generated using the same set of meteorological forcing inputs, without any snow data assimilation.

Table S1. Characteristics of the snow data products used in this study. For the globally available snow products, in addition to SWE, other forcing variables such as precipitation (*P*), air temperature (T_a) and snowfall (*S*) are also used. [1] Liu et al., 2021a; [2] Muñoz-Sabater et al., 2021; [3] Hersbach et al., 2020; [4] Rodell et al., 2004; [5] Gelaro et al., 2017; [6] Kobayashi et al., 2015

Dataset	**Spatial resolution**	**Temporal coverage**	**Temporal resolution**	**Land Surface Model**	**Assimilated snow observations**	**Available variables used in analysis**
HMASR[1] (reference)	1/225° x 1/225°	1999/10 -2017/09	Daily	SSiB3	Fractional snow-covered area from Landsat and MODSCAG	SWE
ERA5-Land[2]	0.1° x 0.1°	1950 - present	Hourly	H-TESSEL	-	SWE, *P, T_a, S*
ERA5[3]	0.25° x 0.25°	1950 - present	Hourly	H-TESSEL	In situ snow depth; IMS snow cover (binary)	SWE, *P, T_a, S*
GLDAS-Noah (0.25°)[4]	0.25° x 0.25°	2000/01 - present	3-hour	Noah	-	SWE, *P, T_a, S*
MERRA2[5]	0.625° x 0.5°	1979 - present	Hourly	Catchment	-	SWE, *P, T_a, S*
JRA-55[6]	0.5625° x 0.5616°	1958 - present	3- or 6-hour	SiB	In-situ snow depth, SSM/I, SSMIS snow cover (binary)	SWE, *P, T_a, S*
GLDAS-Noah (1°)	1° x 1°	2000/01 - present	3-hour	Noah	-	SWE, *P, T_a, S*
GLDAS-VIC (1°)				VIC		
GLDAS-CLSM (1°)				Catchment		

Text S2. Methods: Definition of the snow accumulation season

The snow accumulation season is defined at the pixel scale, from day of water year (DOWY) 1 (t_0) through the pixel-wise peak SWE DOWY (t_{peak}; Figure S1). Defining these quantities at the pixel-scale isolates accumulation-season processes, while doing so at the basin or larger scale inevitably mixes accumulation season and melt season processes due to significant elevational variations within the region examined. Spatial variations in t_{peak} are indicative of seasonal and elevational patterns in climatology, but are also a function of model-specific inputs and process representation.

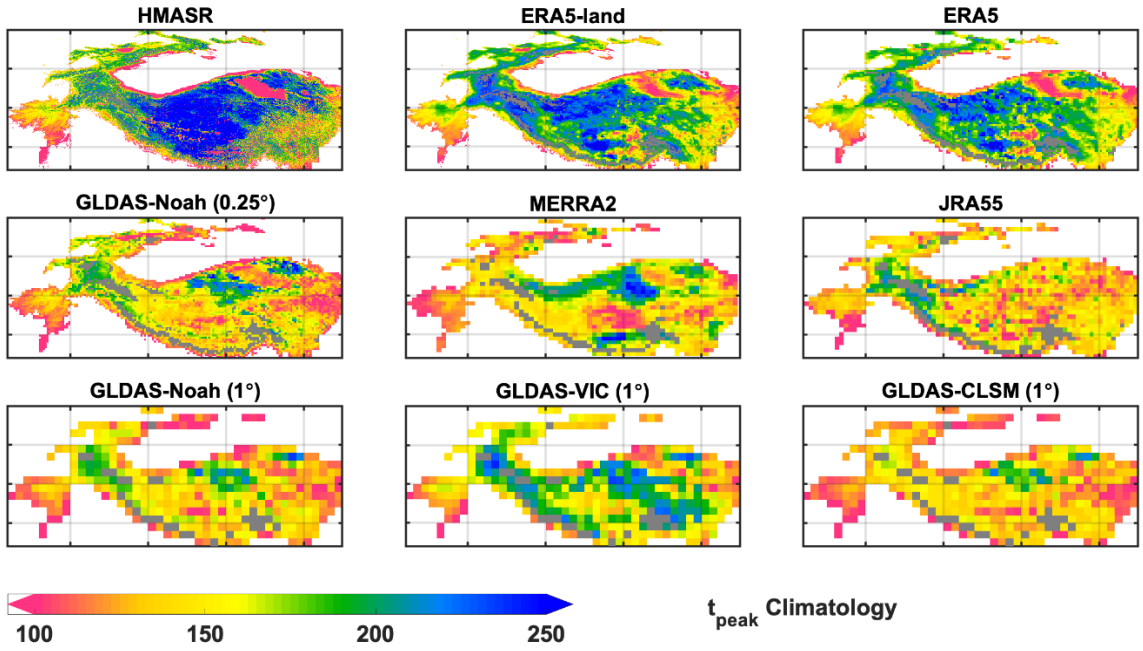

Figure S1. Maps of the 17-year climatology of pixel-wise peak SWE DOWY ($\boldsymbol{t_{peak}}$) for each dataset.

Text S3. Methods: Snow mass balance at the pixel-scale during accumulation season

Snow mass balance at the model pixel scale can be described as the relationship between SWE (denoted as *swe* in m), snowfall (*s*, in m/day) and ablation (*a*, in m/day):

$$\frac{d}{dt}swe = s - a \tag{S1}$$

The snow accumulation season is defined at the pixel scale, from day of water year (DOWY) 1 (t_0) through the pixel-wise peak SWE DOWY (t_{peak}; Figure S2):

$$\int_{t_0}^{t_{peak}} \left[\frac{d}{dt}swe\right] dt = \int_{t_0}^{t_{peak}} [s - a] dt \tag{S2}$$

$$swe_{peak} = s_{acc} - a_{acc} \tag{S3}$$

where swe_{peak} characterizes the net added SWE within the accumulation season at a specific pixel. The s_{acc} and a_{acc} terms denote the cumulative snowfall and snow ablation integrated over the accumulation season. The variables swe_{peak} and s_{acc} are directly obtained from each snow product. Since different LSMs across products represent and handle ablation processes differently, a_{acc} is obtained herein as the difference between s_{acc} and swe_{peak} (similar to Xu et al., 2019):

$$a_{acc} = s_{acc} - swe_{peak} \tag{S4}$$

It should also be noted that while most snow products showed consistency between integrated positive SWE increments and snowfall (Figure 1b in the main text), JRA55 consistently exhibits SWE changes lower than expected relative to snowfall (i.e. data assimilation increments appear to be mostly negative). For this reason, the diagnosed ablation (defined herein as the difference between s_{acc} and swe_{peak}; Equation S4) for JRA55 is likely a mix of model-specific ablation processes and non-negligible data assimilation corrections. This explains why JRA55 has higher snowfall estimates, but among the lower SWE estimates among the datasets in Figure 1b.

Text S4. Methods: Seasonal, ephemeral, and persistent snow masks

As in Liu et al. (2021b), the HMASR dataset is used to derive masks for persistent snow/ice, seasonal snow, and ephemeral (intermittent) snow (Figure S2). The persistent snow mask (derived in Liu et al., 2021b) is used to remove areas that are likely glacierized or with significant carry-over snow storage from one WY to the next. Seasonal and ephemeral snow pixels are distinguished using a threshold of 0.05 m in climatological peak SWE, where the distinction is made due to the expected differences in their accumulation-season characteristics (e.g. seasonal snow lasts longer, ephemeral snow is intermittent with shorter duration, and the latter does not have a distinct accumulation season). Other work uses the Sturm et al. (1995) classification that identifies ephemeral snow as that with the snow duration less than 60 days and snow depth below 50 cm (e.g. Petersky and Harpold, 2018; Wrzesien et al., 2019).

For the purpose of assessing the peak snow storage in HMA, seasonal snow is emphasized in this work. Ephemeral snow is also assessed due to its vast coverage and non-negligible volumetric contribution to the total storage. Both are examined in this work so that the accumulation/ablation processes in the accumulation season are properly characterized for each snow regime. Moreover, areas under 1500 m elevation are screened out within the whole HMA domain and in all three masks (seasonal, ephemeral and persistent snow), to emphasize the focus on areas that are more likely to have snow (above 1500 m elevation).

For consistency, we applied the three HMASR-derived masks to all other datasets, by aggregating them from the original HMASR resolution (~500 m) to the coarser resolution grids in each product (Figure S2). The masked areas were carefully examined to make sure they are comparable across datasets (Table S2). Seasonal snow regimes mainly cover the northwestern mountain regions (dominated by winter westerlies, covering ~23% of the total area), while ephemeral snow mainly covers the vast area in the central and eastern regions (dominated by summer monsoons, covering ~69% of the total area), with the highest mountains covered by persistent snow/ice (covering ~8% of the total area).

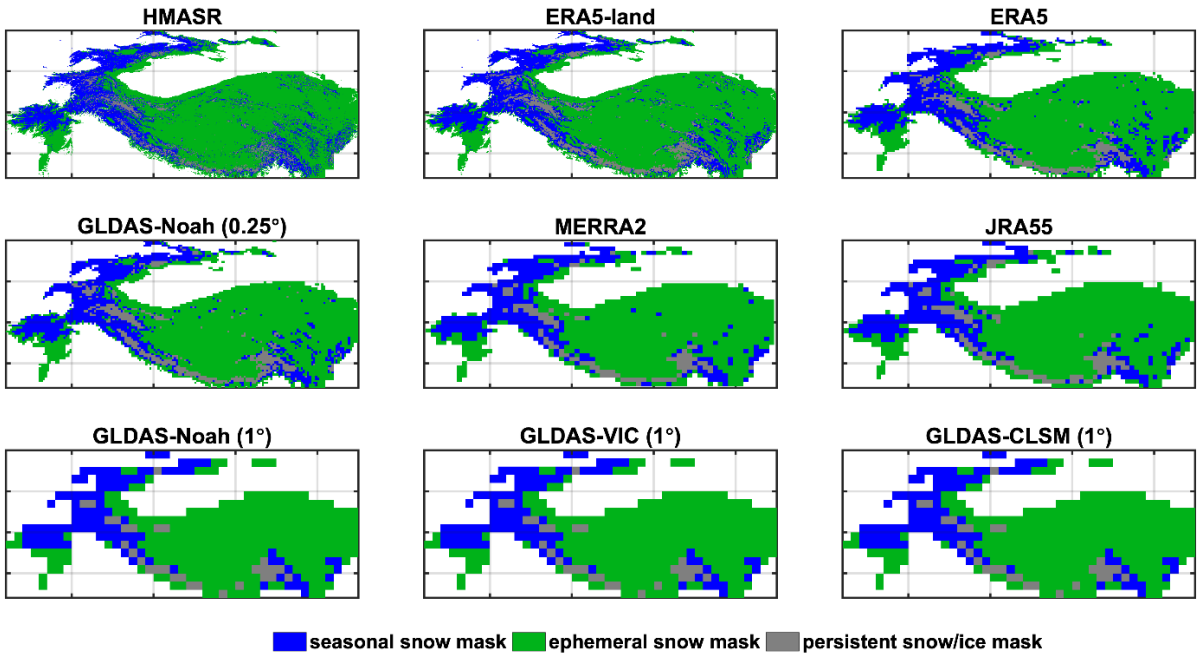

Figure S2. The derived seasonal snow, ephemeral snow, and persistent snow/ice masks shown at the native resolution of each dataset.

Table S2. The total domain area (above 1500 m elevation) and the area of seasonal snow, ephemeral snow, and persistent snow/ice in all datasets.

Dataset	Total Domain Area (above 1500 m elevation) (10^6 km^2)	Seasonal Snow Area (10^6 km^2)	Ephemeral Snow Area (10^6 km^2)	Persistent snow/ice area (10^6 km^2)
HMASR	4.14	1.00	2.88	0.26
ERA5-land	4.13	0.97	2.78	0.38
ERA5	4.11	0.98	2.77	0.36
GLDAS-Noah (0.25°)	4.14	0.87	2.90	0.37
MERRA2	4.10	0.88	2.90	0.32
JRA55	4.14	0.97	2.81	0.35
GLDAS-Noah (1°)	4.15	0.95	2.90	0.30
GLDAS-VIC (1°)	4.15	1.01	2.84	0.30
GLDAS-CLSM (1°)	4.15	1.06	2.79	0.30
Average	4.13	0.97	2.84	0.33
Percentage relative to total area	100%	23%	69%	8%

Text S5. Methods: Spatial and elevational integration

The pixel-scale quantities of swe_{peak}, s_{acc} and a_{acc} are further aggregated to the full HMA domain and at subregional scales, with persistent snow pixels (Text S4; Figure S2) masked out prior to the integration. Spatial integration of these quantities yields the same relationship as Equation (S3):

$$SWE_{peak} = S_{acc} - A_{acc} \quad \text{(S5)}$$

where SWE_{peak} is the pixel-wise peak SWE volume, and S_{acc} and A_{acc} respectively denote the cumulative snowfall and snow ablation volume integrated over the accumulation season. All three quantities are aggregated across the HMA-scale or subregional-scale domain.

Spatial integration over elevation bands is also detailed here (Figure S3). The DEM for each dataset (at the native resolution) is shown for a representative tile 34°N, 66°E in Figure S3a. The hypsometry over the whole domain (Figure S3b) shows how the areal distribution of elevation varies across datasets. For elevational distributions of variables (e.g. SWE_{peak} and S_{acc}), the native DEMs for each dataset were used to integrate into volumes by discretizing elevation bands using intervals of 1000 m (centered on 1500, 2500, 3500, 4500, and 5500 m). Compared with HMASR, all snow product DEMs have less area below 2000 m or above 3500 m, and more area in between (2000 – 3500 m). The hypsometry is generally consistent above 3500 m, and most different around 2500 m across snow products, with GLDAS (1°) showing the highest area, followed by JRA55 and MERRA2, while ERA5 and GLDAS (0.25°) show the least area (yet slightly higher than HMASR).

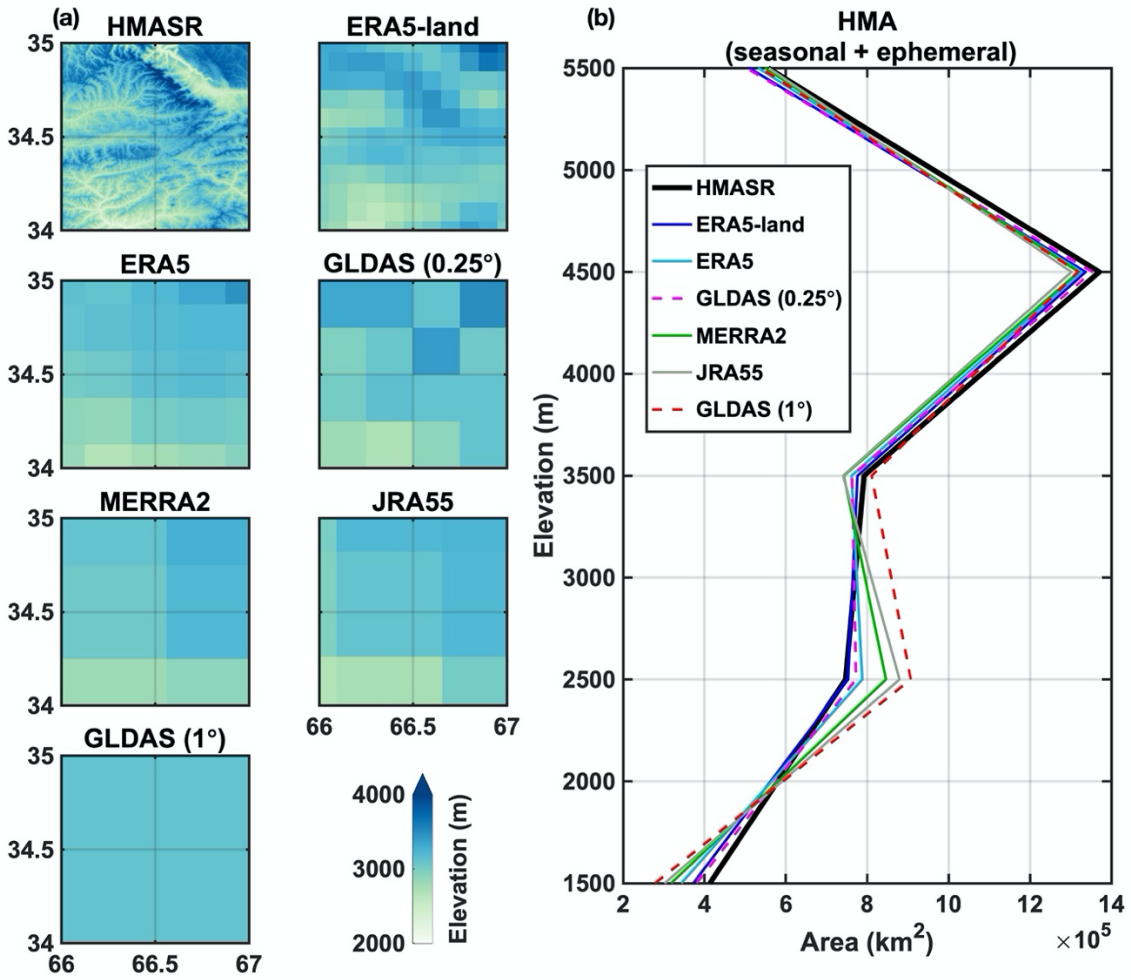

Figure S3. Illustration of dataset-specific **a**) DEMs for a representative tile (34°N, 66°E) at the native resolution and **b**) hypsometry over the HMA domain (masked with seasonal and ephemeral snow areas shown in Figure S1, with persistent snow and areas under 1500 m elevation excluded), integrated over 1000-m elevation bins (centered on 1500, 2500, 3500, 4500, and 5500 m).

Text S6: Methods: Linear regression

As shown in many previous studies, precipitation (in particular snowfall) is often regarded as the key variable affecting peak SWE estimation (Clark et al., 2011; Magnusson et al., 2015; Xu et al., 2019; Cho et al., 2022). Along these lines, we use a simple linear regression to examine the relationship between SWE_{peak} and S_{acc}:

$$SWE_{peak} = \beta * S_{acc} + \varepsilon \quad \text{(S6)}$$

where SWE_{peak} and S_{acc} are available for each snow product and each WY. In the analysis below, the regression is used to examine both global (i.e. across all snow products and WYs) and local (i.e. for a single snow product across all WYs) variations.

The β term is the regression coefficient (slope), and is derived either globally (β_{global}) or locally (β_i). The slope physically represents the fraction of cumulative snowfall that remains in the snowpack at t_{peak}. In the limit of no ablation the slope would be ~1, while the occurrence of accumulation-season ablation will generally lead to values < 1. The ε term is the random noise, which is assumed to be independent of the predictor (S_{acc}). To avoid collinearity, A_{acc} is not explicitly included as a predictor in the linear regression, as it is simply computed as the difference between S_{acc} and SWE_{peak} (Similar to Equation S4). The coefficient of determination (R^2) is often used to measure the goodness of fit for the linear model, and its value can be interpreted as the fraction of the explained variance. The above approach provides a mechanism to determine the relative role of snowfall vs. ablation in contributing to peak snow storage (through the slope) as well as explain the variation in peak storage relative to snowfall.

Text S7. Results: Climatology and uncertainty in HMA-wide peak snow storage

As referenced in the main text, Table S3 shows the 17-year climatology of SWE_{peak} in the eight global snow products, and their percent difference compared with those in HMASR.

Table S3. 17-year climatology of $\boldsymbol{SWE_{peak}}$ and the percent difference in the eight snow products compared to those in HMASR, over the full HMA domain and over the areas with seasonal and ephemeral snow.

	HMA		Seasonal		Ephemeral	
Dataset	$\boldsymbol{SWE_{peak}}$ (km^3)	% difference from HMASR	$\boldsymbol{SWE_{peak}}$ (km^3)	% difference from HMASR	$\boldsymbol{SWE_{peak}}$ (km^3)	% difference from HMASR
HMASR	239	-	210	-	30	-
ERA5-land	341	43%	249	19%	93	210%
ERA5	288	20%	198	-5%	90	200%
GLDAS-Noah (0.25°)	120	-50%	84	-60%	36	20%
MERRA2	54	-77%	35	-83%	18	-38%
JRA55	93	-61%	64	-69%	29	-3%
GLDAS-Noah (1°)	114	-53%	76	-64%	37	25%
GLDAS-VIC (1°)	179	-25%	113	-46%	65	119%
GLDAS-CLSM (1°)	98	-59%	61	-71%	38	26%
Mean (excluding HMASR)	161	-	110	-	51	-
Standard Deviation (excluding HMASR)	102	-	74	-	28	-
Mean Difference	-	-33%	-	-47%	-	70%
Root Mean Square Difference	-	52%	-	58%	-	113%

Text S8. Results: Elevational distribution in the volumetric fraction of S_{acc}, A_{acc} and SWE_{peak} climatology over the full HMA domain

The elevational distribution of S_{acc}, A_{acc} and SWE_{peak} climatology over the full HMA domain is shown in Figure S4, with volumes normalized by total S_{acc} to present the volumetric fraction. Given the significant differences in snowfall across snow products, the normalization reflects how, for the same amount of snowfall, each snow product distributes snowfall across elevation and how that fraction is partitioned into A_{acc} and SWE_{peak}. The elevational distribution over the full HMA domain exhibits a generally consistent pattern with that over the seasonal and ephemeral snow regimes. For convenience, we define the elevation bands centered on 2500 m, 3500 m and 4500 m as low-, mid- and high-elevation herein.

The fractional S_{acc} distribution over elevation is generally consistent across snow products, except that MERRA2 exhibits a slightly higher fraction at low-elevation and a lower fraction at high-elevation. ERA5 and ERA5-land exhibit higher S_{acc} fractions at mid-elevation (5% more than MERRA2) and lower fractions at high-elevation (comparable to MERRA2). The GLDAS products exhibits the lowest fractions at low-elevation (~ 5-8% less than MERRA2) but the highest fractions at high-elevation (~8% more than MERRA2).

The fractional A_{acc} distribution is significantly more distinct across snow products. At low- and mid-elevation, both ERA5-land and GLDAS-VIC stand out as having the lowest fractions, while ERA5 and the other GLDAS products show moderate fractions (8% more than ERA5-land), and MERRA2 shows the highest fraction (20% more than ERA5-land). At high-elevation, ERA5-land and GLDAS-VIC show the least fractional A_{acc}, but ERA5 exhibits a comparable fraction compared to ERA5-land. The other GLDAS products and MERRA2 show the highest fractions (8% more than ERA5-land). The extremely low ablation in ERA5-land and ERA5 at high-elevation is discussed in Hersbach et al. (2020) and is attributed to its single layer snow model not producing enough melt. The other three GLDAS products only exhibit minor difference with ~2% less fractional A_{acc} in GLDAS-Noah (0.25°) and 1% less fractional A_{acc} in GLDAS-Noah (1°) compared to GLDAS-CLSM at low-elevation, but barely exhibit any difference at mid- or high-elevation.

The elevational distribution of fractional SWE_{peak} is a direct result of fractional S_{acc} and A_{acc}. In general, ERA5-land exhibits the highest fractional SWE_{peak}, while MERRA2 has the lowest fraction, primarily because MERRA2 consistently has higher fractional A_{acc}. Their differences are the largest (13%) at mid-elevation where MERRA2 exhibits less fractional S_{acc}, and the smallest (5%) at low-elevation where MERRA2 exhibits more fractional S_{acc}. Compared with ERA5-land, GLDAS-VIC shows ~7% less fractional SWE_{peak} at mid-elevation, but ~6% more at high-elevation, primarily because of the difference in fractional S_{acc} distribution. Again, the other three GLDAS products exhibit a relatively consistent distribution in fractional SWE_{peak}, except for the 0.25° product, which shows a slightly higher fraction (~3%) at mid-elevation due to the fractional S_{acc} difference compared with other products. GLDAS also exhibits more fractional SWE_{peak} than MERRA2, with the largest difference (8%) at high-elevation where GLDAS obtains more fractional S_{acc} but equivalent fractional A_{acc}, and the smallest difference (<1%) at low-elevation where GLDAS exhibits less fractional S_{acc} and less fractional A_{acc}. These highlight the important role of ablation in removing snowfall differently with elevation, leading to a distinct distribution in fractional SWE_{peak} rather than just reproducing the fractional S_{acc} distribution.

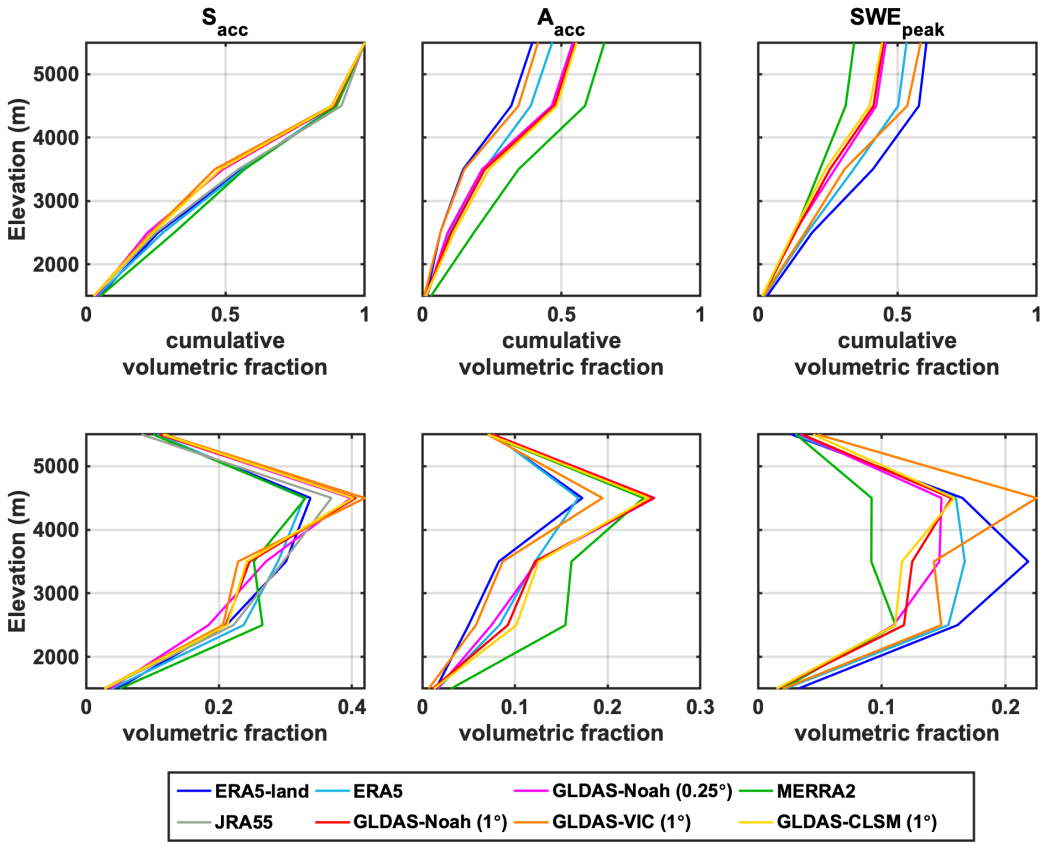

Figure S4. Volumetric fraction of accumulation-season snowfall ($\boldsymbol{S_{acc}}$), ablation ($\boldsymbol{A_{acc}}$) and peak SWE ($\boldsymbol{SWE_{peak}}$), integrated over 1000-m elevation bins (centered on 1500, 2500, 3500, 4500, and 5500 m) over the full HMA domain. The fractional distribution is obtained for each snow product by normalizing the distribution by the product-specific total $\boldsymbol{S_{acc}}$ across all elevations. The top panel displays the cumulative volumetric fraction across elevation bins, and the bottom panel displays the absolute volumetric fraction within elevation bins. Note that the fractional ablation and SWE in JRA55 are not displayed here, due to its diagnosed ablation being overestimated as a result of its snow data assimilation updates.

Text S9. Results: Explanations of peak snow storage variations from accumulation-season snowfall and ablation

As referenced in the main text, Table S4, Figure S5 and Figure S6 presented in this supplementary information are used to explain peak snow storage variations from accumulation-season snowfall and ablation.

Table S4 shows the linear regression statistics between SWE_{peak} and S_{acc} across WYs 2001-2017, with volumes integrated over the full HMA domain, seasonal and ephemeral snow regimes. As introduced in Text S6, regression is performed locally (for each snow product) and globally (across all snow product), with the exception of JRA55, which is not included in the global linear regression, due to its diagnosed ablation being overestimated as a result of its snow data assimilation updates.

Figure S5 shows the linear regression between SWE_{peak} and S_{acc} across WYs 2001-2017, with volumes integrated over the full HMA domain. The snow products are partitioned into two groups (subsets) (subset 1: GLDAS products and MERRA2, subset 2: ERA5 and ERA5-land), based on the notable gap between ERA5 and GLDAS seen from S_{acc}, where the linear statistics are obtained separately within each subset as shown on Figure S5.

Figure S6 shows the linear regression between S_{acc} and P_{acc} (accumulation-season precipitation) across WYs 2001-2017, with volumes integrated over the full HMA domain, to examine how much S_{acc} variations are explained by precipitation vs. rain-snow partitioning across snow products.

Table S4: Linear regression statistics of slope (β) and R^2, from global and local (snow product-specific regressions), where all regressions are statistically significant with p-values < 0.05. Note that JRA55 results are only displayed here (with statistics greyed-out in the table) but not included in the global linear regression due to its diagnosed ablation being overestimated as a result of its snow data assimilation updates.

	Slope ($\boldsymbol{\beta}$)			$\boldsymbol{R^2}$		
	HMA-wide	Seasonal	Ephemeral	HMA-wide	Seasonal	Ephemeral
Global	**0.54**	**0.71**	**0.35**	**0.88**	**0.88**	**0.80**
ERA5-land	0.61	0.83	0.35	0.58	0.94	0.25
ERA5	0.53	0.67	0.36	0.53	0.70	0.32
GLDAS-Noah (0.25°)	0.45	0.59	0.29	0.48	0.76	0.36
MERRA2	0.35	0.46	0.24	0.48	0.62	0.42
JRA55	0.25	0.30	0.17	0.61	0.77	0.33
GLDAS-Noah (1°)	0.45	0.58	0.29	0.46	0.76	0.35
GLDAS-VIC (1°)	0.58	0.76	0.41	0.60	0.83	0.48
GLDAS-CLSM (1°)	0.44	0.55	0.33	0.46	0.66	0.37

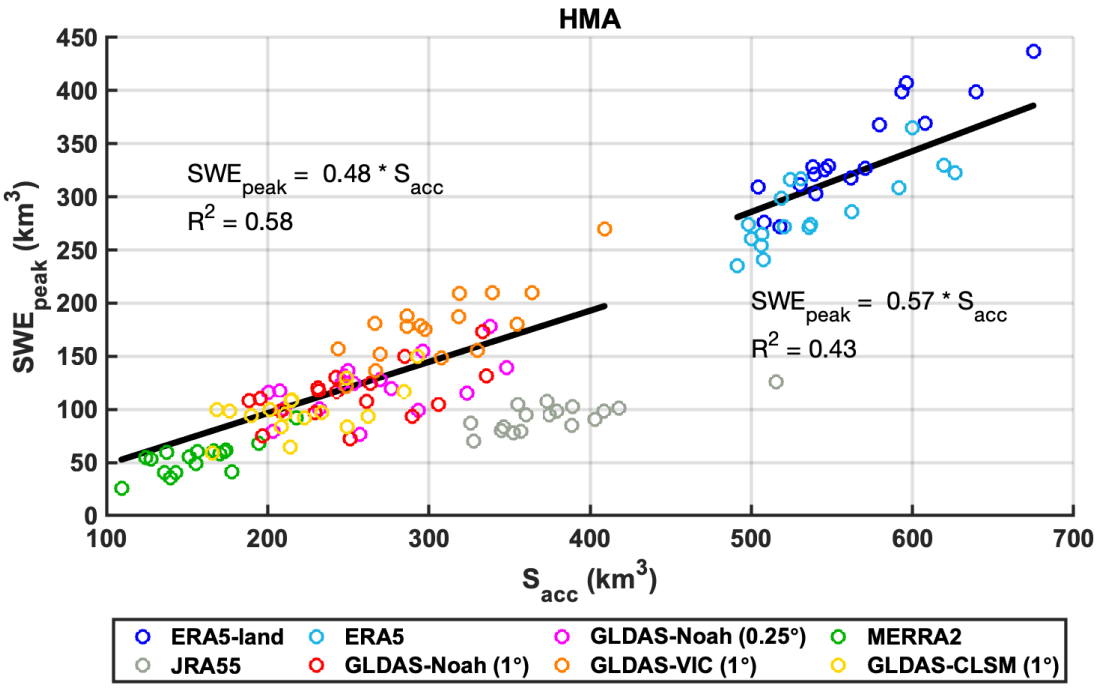

Figure S5. Regression of peak SWE volume ($\boldsymbol{SWE_{peak}}$) and accumulation-season snowfall ($\boldsymbol{S_{acc}}$) across WYs 2001-2017, with volumes integrated over the full HMA domain. Regression is performed over two subsets of datasets (subset 1: GLDAS products and MERRA2, subset 2: ERA5 and ERA5-land).

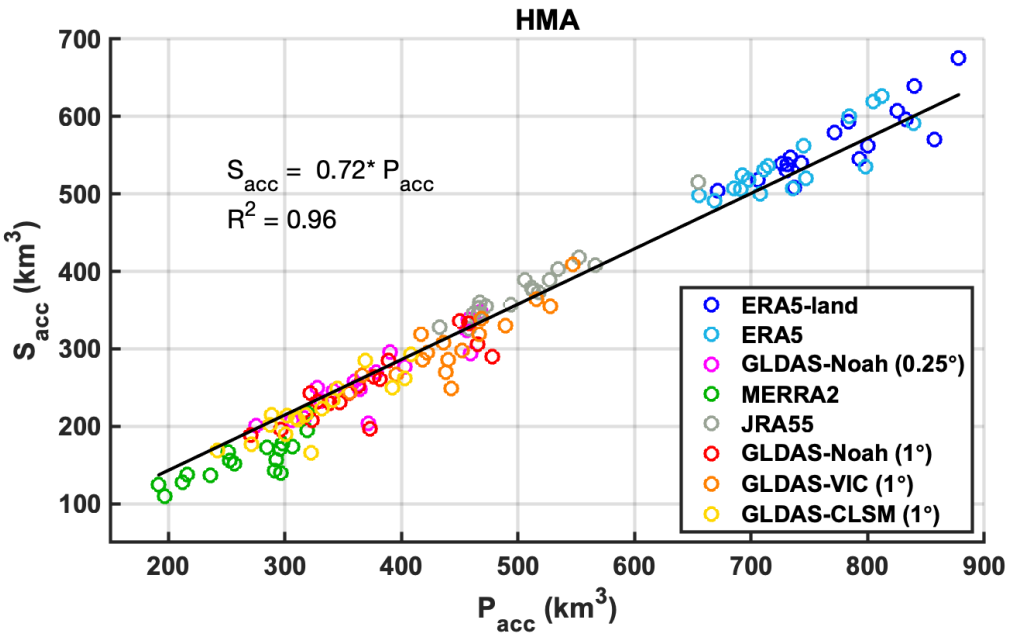

Figure S6. Regression of accumulation-season snowfall ($\boldsymbol{S_{acc}}$) vs. precipitation ($\boldsymbol{P_{acc}}$) across WYs 2001-2017, with volumes integrated over the full HMA domain.

SI references:

Bian, Q., Xu, Z., Zhao, L., Zhang, Y.-F., Zheng, H., Shi, C., Zhang, S., Xie, C., & Yang, Z.-L. (2019). Evaluation and Intercomparison of Multiple Snow Water Equivalent Products over the Tibetan Plateau. *Journal of Hydrometeorology*, *20*(10), 2043–2055. https://doi.org/10.1175/JHM-D-19-0011.1

Cho, E., Vuyovich, C. M., Kumar, S. V., Wrzesien, M. L., Kim, R. S., & Jacobs, J. M. (2022). Precipitation Biases and Snow Physics Limitations Drive the Uncertainties in Macroscale Modeled Snow Water Equivalent. *Hydrology and Earth System Sciences Discussions*, *2022*, 1–22. https://doi.org/10.5194/hess-2022-136

Clark, M. P., Hendrikx, J., Slater, A. G., Kavetski, D., Anderson, B., Cullen, N. J., Kerr, T., Örn Hreinsson, E., & Woods, R. A. (2011). Representing spatial variability of snow water equivalent in hydrologic and land-surface models: A review. *Water Resources Research*, *47*(7). https://doi.org/10.1029/2011WR010745

Gelaro, R., McCarty, W., Suárez, M. J., Todling, R., Molod, A., Takacs, L., Randles, C. A., Darmenov, A., Bosilovich, M. G., Reichle, R., Wargan, K., Coy, L., Cullather, R., Draper, C., Akella, S., Buchard, V., Conaty, A., da Silva, A. M., Gu, W., … Zhao, B. (2017). The Modern-Era Retrospective Analysis for Research and Applications, Version 2 (MERRA-2). *Journal of Climate*, *30*(14), 5419–5454. https://doi.org/10.1175/JCLI-D-16-0758.1

Hersbach, H., Bell, B., Berrisford, P., Hirahara, S., Horányi, A., Muñoz-Sabater, J., Nicolas, J., Peubey, C., Radu, R., Schepers, D., Simmons, A., Soci, C., Abdalla, S., Abellan, X., Balsamo, G., Bechtold, P., Biavati, G., Bidlot, J., Bonavita, M., … Thépaut, J.-N. (2020). The ERA5 global reanalysis. *Quarterly Journal of the Royal Meteorological Society*, *146*(730), 1999–2049. https://doi.org/10.1002/qj.3803

KOBAYASHI, S., OTA, Y., HARADA, Y., EBITA, A., MORIYA, M., ONODA, H., ONOGI, K., KAMAHORI, H., KOBAYASHI, C., ENDO, H., MIYAOKA, K., & TAKAHASHI, K. (2015). The JRA-55 Reanalysis: General Specifications and Basic Characteristics. *Journal of the Meteorological Society of Japan. Ser. II*, *93*(1), 5–48. https://doi.org/10.2151/jmsj.2015-001

Liu, Y., Fang, Y., & Margulis, S.A. (2021a). High Mountain Asia UCLA Daily Snow Reanalysis, Version 1. Boulder, Colorado USA, NASA Snow and Ice Data Center Distributed Active Archive Center. https://doi.org/10.5067/HNAUGJQXSCVU

Liu, Y., Fang, Y., & Margulis, S. A. (2021b). Spatiotemporal distribution of seasonal snow water equivalent in High Mountain Asia from an 18-year \hack\break Landsat–MODIS era snow reanalysis dataset. *The Cryosphere*, *15*(11), 5261–5280. https://doi.org/10.5194/tc-15-5261-2021

Magnusson, J., Wever, N., Essery, R., Helbig, N., Winstral, A., & Jonas, T. (2015). Evaluating snow models with varying process representations for hydrological applications. *Water Resources Research*, *51*(4), 2707–2723. https://doi.org/10.1002/2014WR016498

Muñoz-Sabater, J., Dutra, E., Agustí-Panareda, A., Albergel, C., Arduini, G., Balsamo, G., Boussetta, S., Choulga, M., Harrigan, S., Hersbach, H., Martens, B., Miralles, D. G., Piles, M., Rodríguez-Fernández, N. J., Zsoter, E., Buontempo, C., & Thépaut, J.-N. (2021). ERA5-Land: A state-of-the-art global reanalysis dataset for land applications. *Earth System Science Data*, *13*(9), 4349–4383. https://doi.org/10.5194/essd-13-4349-2021

ONOGI, K., TSUTSUI, J., KOIDE, H., SAKAMOTO, M., KOBAYASHI, S., HATSUSHIKA, H., MATSUMOTO, T., YAMAZAKI, N., KAMAHORI, H., TAKAHASHI, K., KADOKURA, S., WADA, K., KATO, K., OYAMA, R., OSE, T., MANNOJI, N., & TAIRA, R. (2007). The JRA-25 Reanalysis. *気象集誌. 第 2 輯*, *85*(3), 369–432. https://doi.org/10.2151/jmsj.85.369

Petersky, R., & Harpold, A. (2018). Now you see it, now you don't: A case study of ephemeral snowpacks and soil moisture response in the Great Basin, USA. *Hydrology and Earth System Sciences*, *22*(9), 4891–4906. https://doi.org/10.5194/hess-22-4891-2018

Reichle, R. H., Draper, C. S., Liu, Q., Girotto, M., Mahanama, S. P. P., Koster, R. D., & De Lannoy, G. J. M. (2017). Assessment of MERRA-2 Land Surface Hydrology Estimates. *Journal of Climate*, *30*(8), 2937–2960. https://doi.org/10.1175/JCLI-D-16-0720.1

Rodell, M., Houser, P. R., Jambor, U., Gottschalck, J., Mitchell, K., Meng, C.-J., Arsenault, K., Cosgrove, B., Radakovich, J., Bosilovich, M., Entin, J. K., Walker, J. P., Lohmann, D., & Toll, D. (2004). The Global Land Data Assimilation System. *Bulletin of the American Meteorological Society*, *85*(3), 381–394. https://doi.org/10.1175/BAMS-85-3-381

Sturm, M., Holmgren, J., & Liston, G. E. (1995). A Seasonal Snow Cover Classification System for Local to Global Applications. *Journal of Climate*, *8*(5), 1261–1283. https://doi.org/10.1175/1520-0442(1995)008<1261:ASSCCS>2.0.CO;2

Wrzesien, M. L., Pavelsky, T. M., Durand, M. T., Dozier, J., & Lundquist, J. D. (2019). Characterizing Biases in Mountain Snow Accumulation From Global Data Sets. *Water Resources Research*, *55*(11), 9873–9891. https://doi.org/10.1029/2019WR025350

Xu, Y., Jones, A., & Rhoades, A. (2019). A quantitative method to decompose SWE differences between regional climate models and reanalysis datasets. *Scientific Reports*, *9*(1), 16520. https://doi.org/10.1038/s41598-019-52880-5